

Cold electron beams from cryocooled, alkali antimonide photocathodes

L. Cultrera,* S. Karkare, H. Lee, X. Liu, I. Bazarov, and B. Dunham

*Cornell Laboratory for Accelerator-Based Science and Education,
Cornell University, Ithaca, New York 14853, USA*

(Received 2 February 2015; published 30 November 2015)

In this paper we report on the generation of cold electron beams using a Cs₃Sb photocathode grown by codeposition of Sb and Cs. By cooling the photocathode to 90 K we demonstrate a significant reduction in the mean transverse energy validating the long-standing speculation that the lattice temperature contributes to limiting the mean transverse energy or intrinsic emittance near the photoemission threshold, opening new frontiers in generating ultrabright beams. At 90 K, we achieve a record low intrinsic emittance of 0.2 μm (rms) per mm of laser spot diameter from an ultrafast (subpicosecond) photocathode with quantum efficiency greater than 7×10^{-5} using a visible laser wavelength of 690 nm.

DOI: 10.1103/PhysRevSTAB.18.113401

PACS numbers: 41.75.Fr, 07.77.Ka, 79.60.Dp

I. INTRODUCTION

The quest for photocathodes that generate electron beams with increased brightness to drive x-ray free electron lasers (FEL) [1], energy recovery linacs (ERL) [2], electron cooling of hadron beams [3], inverse Compton scattering [4], and ultrafast electron diffraction (UED) [5] experiments has recently received much attention from the scientific community, resulting in a stronger interaction between accelerator and solid state physicists trying to identify suitable materials with improved performance for future accelerators and novel applications [6].

From the point of view of the electron source for an accelerator device, the photocathode has to satisfy several, often conflicting, requirements: high quantum efficiency (QE); low intrinsic emittance or mean transverse energy (MTE); prompt response time; and photocathode longevity. As of today no photocathode material is able to fulfill all these requirements and application specific tradeoffs have to be made to select an acceptable photocathode material.

High QE is important mostly when defining the specifications for the drive laser: higher QE means that less laser power is needed for the same extracted beam current. For high current (~ 100 mA) applications, like ERL's [2] and electron cooling [3], QE's of a few percent or more in the visible range of the spectrum are needed in order to maintain the average laser power within a few tens of Watts [2]. However, for most other applications such as single pass FEL's or UED setups, where the current requirement is in the 100 μA range or lower [1] and/or the maximum charge per bunch extracted should be

kept small enough to avoid space charge emittance degradation QE in the 10^{-5} range in the visible or UV light is acceptable. Along with sufficient QE, most accelerator applications require photocathodes to have a subpicosecond response time and robustness to vacuum conditions in order to operate without significant QE degradation.

For a given bunch charge, the one-dimensional maximum electron beam brightness achievable from the photoemission source depends only on the MTE and the electric field at the cathode surface [7–9]. The transverse coherence length, which sets the upper limit to the unit cell size of the crystal that can be imaged using UED setups, depends inversely on the intrinsic emittance [5]. The intrinsic emittance is determined by the laser beam size and the MTE of the emitted electrons through the following relations under the assumption of isotropic emission with no correlation between position and momentum:

$$\varepsilon_{n,x} = \sigma_{l,x} \frac{\sqrt{\langle p_x^2 \rangle}}{m_e c} = \sigma_{l,x} \sqrt{\frac{\text{MTE}}{m_e c^2}}, \quad (1)$$

where $\varepsilon_{n,x}$ is the rms normalized transverse emittance in the x plane, $\sigma_{l,x}$ is the rms laser spot size, $\langle p_x^2 \rangle$ the transverse momentum variance, m_e the electron mass, and c is the speed of light. The intrinsic emittance here defined is a characteristic of cathode material properties and surface geometry and does not include space charge effect of generated electron beam.

Lowering the MTE will increase the beam brightness for FELs and ERLs as well as the transverse coherence length for UED extending the frontiers of these applications.

Obtaining transverse coherence on the order of 10 nm in a beam waist of 100 micron to perform UED of large unit cells like those of protein crystals requires electron beam normalized emittances of 0.004 μm or better [10]. Most of the photocathodes used today provide electron beams with MTEs of a few hundred meV that make it very difficult if

*Corresponding author.
lc572@cornell.edu

Published by the American Physical Society under the terms of the Creative Commons Attribution 3.0 License. Further distribution of this work must maintain attribution to the author(s) and the published article's title, journal citation, and DOI.

not practically impossible generating electron bunches with such low emittances.

The question of the lowest MTE achievable is an important basic question at the interface of solid state and beam physics. Disorder induced heating of electrons after emission theoretically limits MTEs to 1–2 meV [11]. The smallest measured MTEs are close to 25 meV (which corresponds to the room temperature, 300 K) from GaAs activated using Cs and NF_3 [12] and from antimony films [13]. However, GaAs cathodes have a very long response time under infrared illumination and antimony films have extremely low QE ($<10^{-6}$ in the UV range) near the threshold making them impractical for ultrafast accelerator applications.

A number of experiments are dedicated to develop superconducting radio frequency electron guns but there are still few experimental data related the operation of photocathodes at cryogenic temperatures [14]. One attempt of operating photocathodes at cryogenic temperature was performed using GaAs [15] cooled to 90 K. The electron beam properties were studied using a dedicated electron energy analyzer [16] but the results showed that at 90 K MTEs of about 75 meV were achieved (corresponding to about 900 K) because of the long tails on the electron energy distribution. Authors claimed that if a longitudinal energy filter is used to cut off electrons with smaller longitudinal energies, MTEs of 5–7 meV might be obtained from the cryocooled GaAs. While it is always conceptually possible to filter out lower energy electrons, this is less than ideal because a practical realization of the scheme is not trivial. For example, the proposed scheme involving a longitudinal energy filter has not been realized to date nor adopted for use in a high voltage dc or rf gun due to practical limitations. Thus, the quest for low emittance photocathodes to generate high brightness electron beam continues.

In this paper we report on MTE of photoelectrons from a Cs_3Sb cathode at room temperature and at a cryogenic temperature of 90 K generated with light at 690 nm. At room temperature photoelectrons have MTE of 40 meV (460 K) with a QE in the 10^{-3} range and at 90 K a record low MTE of 22 meV (260 K) with a QE of 7×10^{-5} under low electric fields of ~ 100 V/m. Our results not only show that Cs_3Sb is a cathode able to generate low MTE electron beams for FEL and UED applications, but also that MTEs obtained from these cathodes, when operated near threshold, are indeed strongly affected by the lattice temperature and reducing the latter can open new frontiers in generating ultrabright electron beams.

II. RESULTS AND DISCUSSION

The experiments have been performed at the photocathode laboratory at Cornell University where the UHV installation has been recently upgraded with a compact high voltage (up to 20 kV) photoelectron gun and a beam

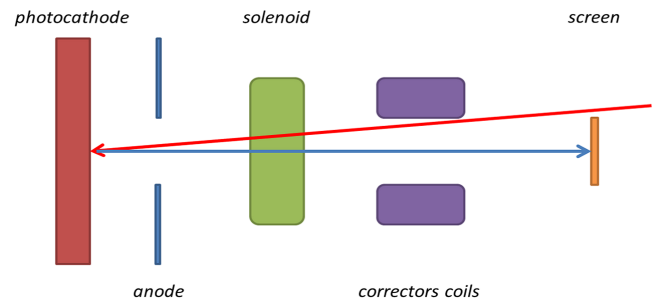


FIG. 1. TEMeter scheme: laser (red) and electron beam (blue) paths are indicated. Typical cathode to anode distance is 4 mm while anode to screen distance is about 25 cm.

line, which includes a solenoid and two pairs of corrector coils (Fig. 1) [17]. We'll refer to this electron gun setup with the name of transverse energy meter (TEMeter) from now on.

The photocathode holder is connected to a liquid nitrogen reservoir, allowing the cooling of the photocathode from room temperature down to ~ 90 K. The 50 mm stainless steel circular anode has a 12 mm diameter hole allowing light generated using laser diodes or by an optical system comprising a lamp and a monochromator be sent to the photocathode surfaces through a UHV window with $\sim 6^\circ$ angle with respect to the axis of the electron gun. Electrons are accelerated by the electric field generated between the negatively biased photocathode surface and the electrically grounded anode, and are sent onto a Ce-doped yttrium-aluminum-garnet (YAG) scintillating screen coated with 7.5 nm of titanium to prevent surface charge accumulation. A CCD camera is used to image and measure the beam size.

A Cs_3Sb cathode has been grown on a *p*-doped Si(100) substrate while cooling from 130°C to 50°C , by coevaporating Sb and Cs with respective fluxes of 3×10^{11} and 1×10^{12} atoms $\text{cm}^{-2} \text{s}^{-1}$ [see Fig. 2(a)] until the QE reached a plateau at 0.05 at 532 nm [see Fig. 2(b)].

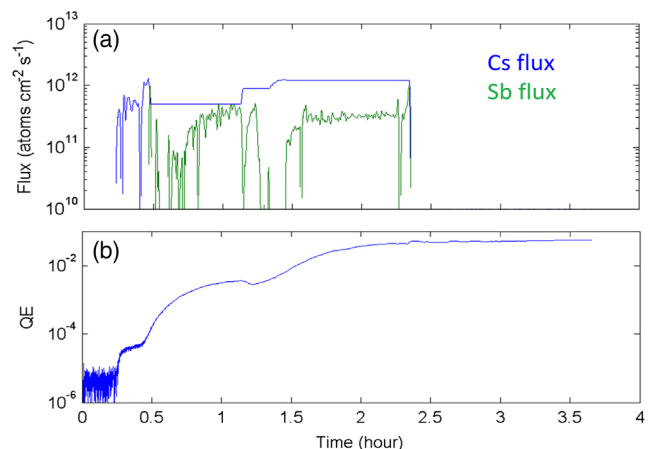


FIG. 2. (a) Fluxes of Cs and Sb vapors and (b) QE at 532 nm during the growth of the Cs_3Sb photocathode.

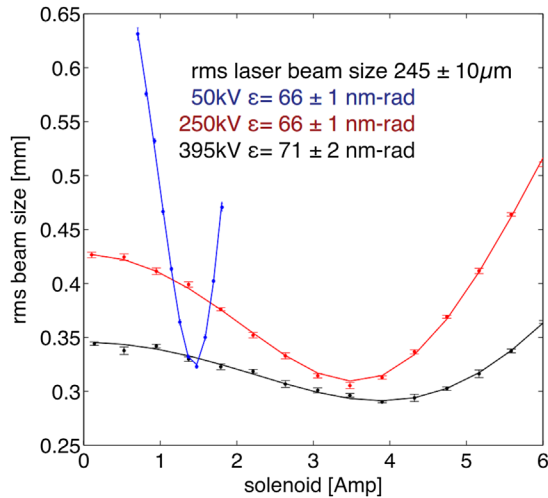


FIG. 3. Electron beam size is measured as a function of the focusing solenoid current of the Cornell-ERL injector prototype high voltage dc gun for three different gun voltages. From the solenoid scan fit the emittance of the beam is retrieved.

The cathode was then moved from the growth chamber to the high voltage (400 kV) electron gun of the Cornell-ERL injector prototype [18] under UHV by using a vacuum suitcase.

QE and intrinsic emittance at 690 nm were measured at room temperature using a laser diode and the solenoid scan technique (Fig. 3) as described in Ref. [19].

Results are reported in Fig. 4 as a function of the gun voltage: while QE is seen to increase from 7.5×10^{-4} to 1.6×10^{-3} due to the Schottky lowering of the work function, MTEs deduced from the beam emittances do not show any noticeable field dependence.

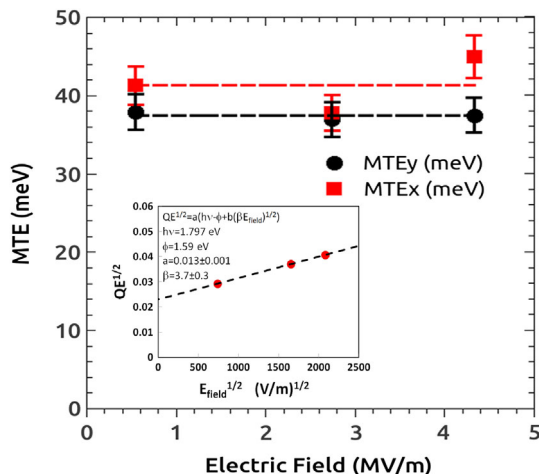


FIG. 4. Cs_3Sb photocathode MTE at 690 nm as obtained from measurements in the injector dc gun. The inset shows the QE fit obtained using Eq. (2) and the retrieved values for a and β . The photoemission threshold used in the fit has been derived from spectral response at room temperature to be 1.59 eV.

QE dependence on the applied electric field can be expressed as [20]

$$QE = a(hv - \phi + b\sqrt{\beta E})^2, \quad (2)$$

where a is a material dependent constant, $h\nu$ is the photon energy, ϕ is the threshold energy for the photoemission, b is defined as $b = \sqrt{e/4\pi\epsilon_0}$, E is the applied electric field and β its enhancement factor. β is deduced from a linear fit of $QE^{0.5}$ as a function of $E^{0.5}$ resulting to be 3.7.

The cathode was then moved back to the photocathode laboratory using the vacuum suitcase and once installed into the TEMeter, it was subjected to few cycles of cooling to cryogenic temperatures (90 K) and back to room temperature (300 K). Intrinsic emittance was estimated using two different methods: the solenoid scan and the free expansion of the electron beam. Data analysis is performed by means of linear optics transfer matrices as illustrated in Ref. [19] and for the free expansion method the solenoid field is set to zero.

Intrinsic emittances were determined using the solenoid scan technique with an rms laser spot size of 60 ± 3 and $64 \pm 3 \mu\text{m}$ respectively for the x and the y direction, using photocurrent intensities in the range of 1 to 2 nA to avoid space charge and for three different gun voltages (5, 7 and 9 kV) corresponding the electric field gradients of 0.88, 1.23 and 1.58 MV/m at 300 and 90 K (examples showing the solenoid scan fit for different gun voltages at 300 K are reported in Fig. 5).

From the linear fit reported in Fig. 6 it is deduced that the MTEs of the electron beam at 300 K and at 90 K are of 40 ± 2 and $22 \pm 1 \text{ meV}$ respectively. The agreement between measurements performed at room temperature in the TEMeter and in the ERL injector prototype dc gun is noteworthy.

Solenoid scan measurements with laser spot size larger than $60 \mu\text{m}$ rms have been found to be affected from

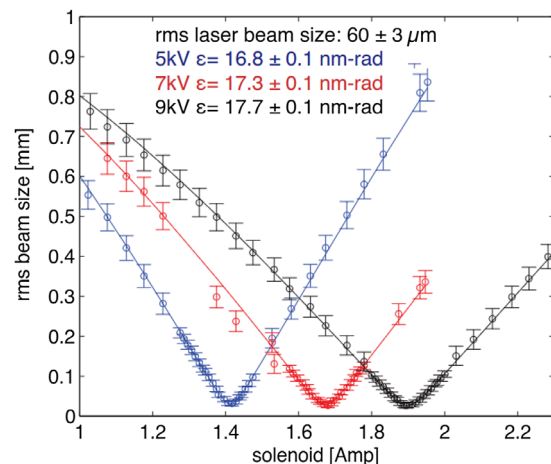


FIG. 5. Solenoid scan measurement taken in the TEMeter at three different gun voltages.

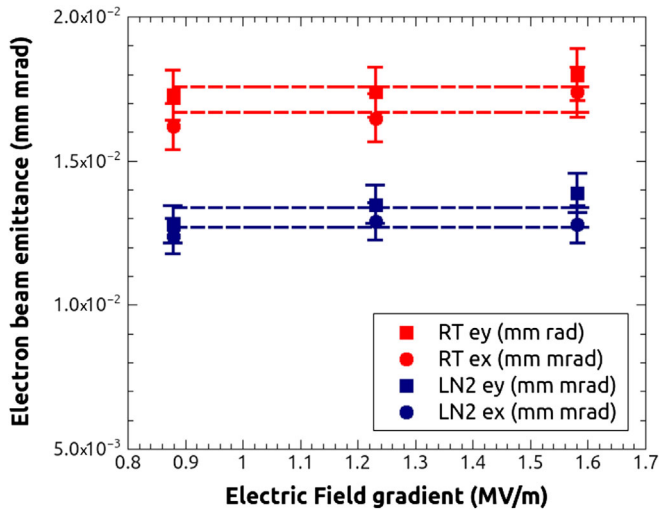


FIG. 6. Solenoid scan measured normalized emittance in the TEMeter at 300 K (red) and at 90 K (blue).

solenoid aberration most likely due to a relatively large electron beam size inside the solenoid magnetic field. For these reasons we performed additional measurements by allowing the electron beam freely expanding using different laser beam sizes and for electric field intensities at the cathode surface varying between 0.5 and 3.4 MV/m.

Two measurements taken at 300 and 90 K with an rms laser spot size of 60 μm are reported in Fig. 7.

Results of the measurements are summarized in Fig. 8 where the emittance of the beam is reported as a function of the initial laser spot size at the cathode surface.

From the linear fit of the beam normalized emittance as a function of the laser beam spot size reported in Fig. 8 the intrinsic emittance of $0.274 \pm 0.006 \mu\text{m}/\text{mm rms}$ ($38 \pm 2 \text{ meV}$) and $0.209 \pm 0.006 \mu\text{m}/\text{mm rms}$ ($22 \pm 1 \text{ meV}$) are estimated at 300 and 90 K respectively.

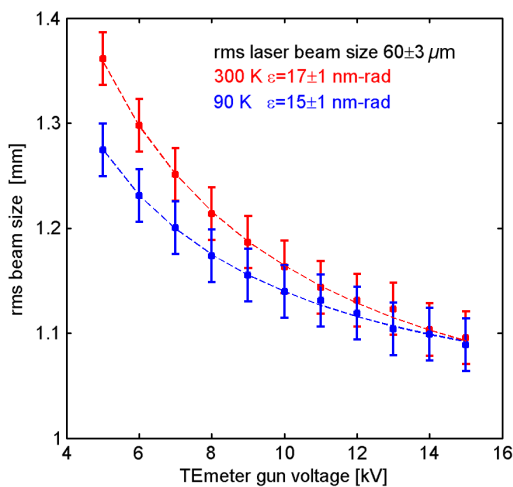


FIG. 7. Electron beam size as measured at the YAG screen on the TEMeter as a function of the gun voltage. From the fit of the data intrinsic emittance of the beam can be retrieved.

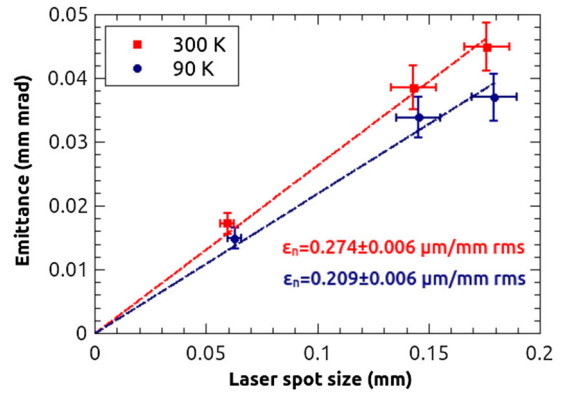


FIG. 8. Intrinsic emittance is deduced from the linear fit of the beam emittances as a function of laser spot size.

Using a bias of -18 V applied to the Cs_3Sb cathode and variable wavelength light from the monochromator the spectral response was measured at both temperatures and reported in Fig. 9. Schottky effect contributions to this measurement are negligible.

Extrapolation of spectral response data allows estimating the photoemission threshold ϕ which within our experimental sensitivity was ~ 1.59 and $\sim 1.72 \text{ eV}$ at 300 and 90 K respectively.

In a very simple model assuming isotropic photoemission with electron energies uniformly distributed in the interval 0 and $h\nu - \phi$ it can be shown that MTE simply reduces to $(h\nu - \phi)/3$ [19]. The predictions of this simple model yield expected values for MTEs of ~ 70 and $\sim 25 \text{ meV}$ for 300 and 90 K respectively for photoelectrons generated using 690 nm photons. Including the Schottky work function lowering scaled by the field enhancement coefficient obtained from QE measurement in the photoinjector gun electric field dependence is expected on MTEs and values as large as $\sim 115 \text{ meV}$ should be observed at 300 K and at 3.4 MV/m. In addition, it is known that the electron beam intrinsic emittance can be degraded by the cathode surface roughness [21–23]. This whole picture looks in contrast with our smaller measured MTEs indicating that a model simply scaled on electrons excess energy cannot explain our experimental result.

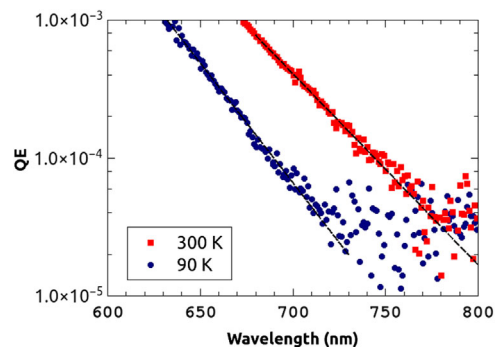


FIG. 9. Spectral response at 300 and 90 K.

Already in 1958, Spicer observed photoemission from alkali antimonide photocathodes illuminated with photons having energies lower than the sum of the band gap (E_g) and electron affinity (E_a) [24]. This observation was interpreted as photoemission from filled donor levels lying near the Fermi level within the gap of the semiconductor. The number of electrons filling these states and contributing to the photoemission process at photon energies lower than the $E_g + E_a$ (~ 1.9 eV) level is strongly related to the temperature of the sample through the Fermi-Dirac distribution. Spicer also observed that, as expected from its interpretation, at cryogenic temperatures the QE of the alkali antimonides photocathodes strongly decreased because of the reduction of the number of electrons filling these donor levels with energies large enough to be excited above the photoemission threshold [24]. Our observation of QE decreasing with reducing temperature is consistent with these results.

A recent model, which includes the effect of the finite temperature on the Fermi-Dirac distribution of the electrons in metals, shows that the intrinsic emittance due to photoelectrons can be expressed as [25]

$$\epsilon_{n,x} = \sigma_{l,x} \sqrt{\frac{kT}{m_e c^2}} \sqrt{\frac{\text{Li}_3\{-\exp[\frac{e}{kT}(hv - \varphi)]\}}{\text{Li}_2\{-\exp[\frac{e}{kT}(hv - \varphi)]\}}}, \quad (3)$$

where T represents the temperature of the electron distribution that is assumed in equilibrium with the lattice temperature and Li_n is a poly-logarithm function defined as [25]

$$\text{Li}_n(z) = \frac{(-1)^{n-1}}{(n-2)!} \int_0^1 \frac{1}{t} \log(t)^{n-2} \log(1-zt) dt. \quad (4)$$

The presence of filled donor states within the energy gap allows us to use the same formula to estimate the emittance and hence the MTE of electron beam generated during our measurements. In our experimental conditions the photon energy (~ 1.8 eV) is smaller than the sum of energy gap and electron affinity of the material (~ 1.9 eV) and under these circumstances the ratio of the two poly-logarithm functions in expression (3) tends to 1, thus the measured MTE in the absence of other effects should equal kT yielding MTEs of 25 and 8 meV for cathode temperature of 300 and 90 K respectively. This result does not depend on the electron affinity as long as the photon energy is much smaller than the effective work function, which includes the Schottky contribution.

Figure 10 reports the MTEs calculated from Eq. (3) at room temperature (continuous red line) and at 90 K (continuous blue line) for the work function value of $\varphi = E_g + E_a = 1.9$ eV [24]. Measured MTEs at room temperature (red dots for MTEs measured in the injector gun, red

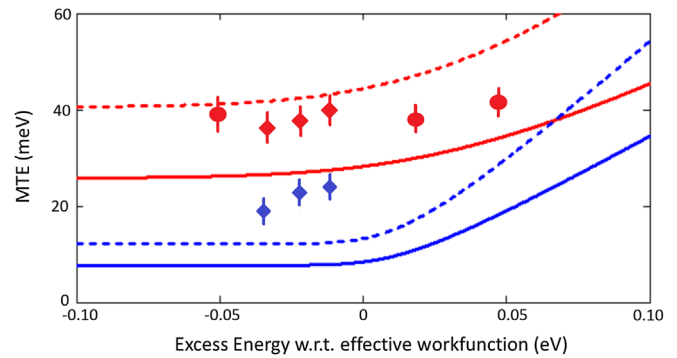


FIG. 10. Electron beam MTEs derived from Eq. (3) at room temperature and 90 K (continuous red and blue line respectively), and MTEs scaled using roughness parameters from Ref. [25] and Eq. (6). Experimental MTEs derived from our beam emittance measurements are also reported: Red dots are measurements in the high voltage gun of the injector at room temperature; diamonds are measurements in the TEMeter at room temperature (red) and 90 K (blue).

diamonds for TEMeter measurements) and at 90 K (blue diamonds) are also shown as a function of the excess energy which is calculated as the difference between the photon energy (1.797 eV) and the effective work function which includes the Schottky lowering and the electric field enhancement coefficient derived from QE measurement in the injector dc gun.

MTEs values measured at 300 and 90 K are larger than the values predicted by Eq. (3). We believe this discrepancy is due to an emittance growth caused by photocathode surface roughness. The scientific community is attempting to address the question of how the roughness affects the intrinsic emittance of a photocathode surface and several models have been proposed in recent years to describe this phenomenon [21–23]. Some of these models indicate that the intrinsic emittance contributions due to the surface roughness can be due to a simply geometrical effect due to the relative orientation of local surfaces from where the electron emission takes place and to an increase of transverse momentum due to transverse electric field components induced by surface roughness. The latter component is usually dependent on the electric field intensity while the former is usually only dependent on the geometry of the surface.

If we consider a simplified two-dimensional roughness model like in Ref. [23],

$$z(x) = a \cos\left(2\pi \frac{x}{\lambda}\right), \quad (5)$$

where a is the amplitude and λ the period of the surface roughness the intrinsic emittance increase $\epsilon_{\text{th},2D}$ due only to the geometry of the surface can be expressed as

$$\varepsilon_{\text{th},2D} \leq \varepsilon_{\text{th}} \sqrt{1 + 6 \left(\frac{\pi a}{\lambda} \right)^2}. \quad (6)$$

The surface of alkali antimonide cathodes has been reported to have a roughness on the order of 25 nm rms with a period of 100 nm [26]. For such surface roughness parameters the square root terms are about equal to 2. We like to stress that the photocathode surface morphology depends on the performed growth procedures and the one obtained with our growth conditions is likely to differ from the one reported in Ref. [26].

If we use the results from Eq. (6) to scale the MTEs expected from Eq. (3) as a function of the estimated electron excess energy we obtain the dashed curves reported in Fig. 10 for room temperature (red dashed line) and 90 K (blue dashed line). The measurements at room temperature are within the upper limit predicted by the simplified emittance growth estimate described by Eq. (6) for a surface morphology similar to the one reported in Ref. [26]. On the other hand, our measurements at 90 K indicate that electron beams with subroom equivalent temperature are achieved but the MTE's obtained values (22 meV) are outside the limits predicted for cryogenic temperatures. The failure of this simple model is not surprising. Dedicated measurements which include the mapping of the actual photocathode surface morphology, MTE and QE at different wavelength, electric field intensity and temperature have to be performed in order to provide a complete detailed data set that can be used to validate a modeling of the intrinsic emittance of photocathodes.

III. CONCLUSIONS

Exploring the photoemission properties of an alkali antimonide photocathode near the emission threshold with visible light at 690 nm and at cryogenic temperatures we have demonstrated that subroom-temperature electrons ($\sim 0.2 \mu\text{m}/\text{mm}$ rms) can be produced with QE (at least 7×10^{-5}) comparable to that of commonly used metals, which, however, require UV excitation light. Electron beams brightness can be improved using alkali antimonides as compared to the metal photocathodes having similar QE but necessitating ultraviolet photons to overcome a larger work function. The copper cathode operating in the LCLS photoinjector has a typical QE of 1×10^{-4} and an intrinsic emittance of $\sim 0.9 \mu\text{m}/\text{mm}$ rms when illuminated with UV light at 253 nm [27]. Also, MTE's between ~ 1 and ~ 20 meV can be achieved using magneto-optical trapping and excitation of Rb atoms as described in [28], but due to practical limitations in achieving higher densities of Rb atoms within the interaction region with the laser beams, the charge per bunch so far has been limited to few tens of fC. Recent results on alkali antimonide photocathodes of the NaKSb type already indicated that these photocathodes

can provide reduced MTE if operated near threshold at expenses of QE [29]. The results here reported indicate that further decrease on the MTE of the electron beam can be obtained by reducing the lattice temperature by cryocooling the Cs₃Sb photocathode, the cooling yields also reduced QEs of the photocathode operated with photons near threshold but the measured values at 690 nm are still larger than most of the metallic photocathodes commonly used in photoguns.

In summary, we have reported on the generation photoelectrons beams with subroom-temperature MTE from Cs₃Sb photocathodes suitable for applications requiring ultrabright and ultrashort bunches. Though the photoemission response time of the photocathode was not characterized at the used wavelength of 690 nm, it is expected to be ps-scale or smaller. This expectation is due to both the small thickness of the photocathode film (10's of nm), as well as the use of alkali antimonide photocathodes in streak cameras with sub-ps resolution in this wavelength range [30]. Even without the cryogenic cooling, the beam brightness is better than previously demonstrated photocathodes. We believe that the surface roughness is a noticeable contributor to the transverse momentum spread of the electrons for this type of photocathodes. We found that a detailed description of the emittance increase beyond the limits induced by the lattice temperatures requires a complete set of measurements (surface morphology, QE and MTE as a function of wavelength and electric field gradient) that have to be performed for the same photocathode in order to provide sufficient data for the model validation. The cooling of the photocathode to even lower temperatures than the one here reported may eventually lead to intrinsic emittances and MTEs of a few meV especially if the cathode surface roughness contribution to emittance growth can be minimized. Another important point to investigate is the emittance increase at higher accelerating fields (10's to 100 MV/m), which is outside our present experimental capabilities.

ACKNOWLEDGMENTS

This work has been funded by the NSF under Grants No. PHY-1416318, No. DMR-0807731 and by the DOE under Grant No. DE-SC0014338.

-
- [1] W. Ackermann *et al.*, *Nat. Photonics* **1**, 336 (2007).
 - [2] S. M. Gruner, D. Bilderback, I. Bazarov, K. Finkelstein, G. Krafft, L. Merminga, H. Padamsee, Q. Shen, C. Sinclair, and M. Tigner, *Rev. Sci. Instrum.* **73**, 1402 (2002).
 - [3] I. Ben-Zvi *et al.*, *Nucl. Instrum. Methods Phys. Res., Sect. A* **532**, 177 (2004).
 - [4] S. Boucher, P. Frigola, A. Murokh, M. Ruelas, I. Jovanovic, J. B. Rosenzweig, and G. Travish, *Nucl. Instrum. Methods Phys. Res., Sect. A* **608**, S54 (2009).

- [5] T. Van Oudheusden, E. F. de Jong, S. B. van der Geer, W.P.E.M. Op 't Root, O. J. Luiten, and B. J. Siwick, *J. Appl. Phys.* **102**, 093501 (2007).
- [6] D. H. Dowell, I. Bazarov, B. Dunham, K. Harkay, C. Hernandez-Garcia, R. Legge, H. Padmore, T. Rao, J. Smedley, and W. Wan, *Nucl. Instrum. Methods Phys. Res., Sect. A* **622**, 685 (2010).
- [7] I. V. Bazarov, B. M. Dunham, and C. K. Sinclair, *Phys. Rev. Lett.* **102**, 104801 (2009).
- [8] C. Gulliford, A. Bartnik, I. Bazarov, L. Cultrera, J. Dobbins, B. Dunham, F. Gonzalez, S. Karkare, H. Lee, H. Li, Y. Li, X. Liu, J. Maxson, C. Nguyen, K. Smolenski, and Z. Zhao, *Phys. Rev. ST Accel. Beams* **16**, 073401 (2013).
- [9] C. Gulliford, A. Bartnik, I. Bazarov, B. Dunham, and L. Cultrera, *Appl. Phys. Lett.* **106**, 094101 (2015).
- [10] C. Gulliford, A. Bartnik, J. M. Maxson, and I. Bazarov, Multiobjective optimizations of ultrafast electron diffraction setups (to be published).
- [11] J. M. Maxson, I. V. Bazarov, W. Wan, H. A. Padmore, and C. E. Coleman-Smith, *New J. Phys.* **15**, 103024 (2013).
- [12] I. V. Bazarov, B. M. Dunham, Y. Li, X. Liu, D. G. Ouzounov, C. K. Sinclair, F. Hannon, and T. Miyajima, *J. Appl. Phys.* **103**, 054901 (2008).
- [13] J. Feng, J. Nasiatka, W. Wan, T. Vecchione, and H. A. Padmore, *Rev. Sci. Instrum.* **86**, 015103 (2015).
- [14] J. Teichert, in *Proceedings of IPAC 2014, Dresden, Germany, 2014* (JACoW, Geneva, Switzerland, 2014), p. 4085.
- [15] D. A. Orlov, U. Weigel, D. Schwalm, A. S. Terekhov, and A. Wolf, *Nucl. Instrum. Methods Phys. Res., Sect. A* **532**, 418 (2004).
- [16] D. A. Orlov, M. Hoppe, U. Weigel, D. Schwalm, A. S. Terekhov, and A. Wolf, *Appl. Phys. Lett.* **78**, 2721 (2001).
- [17] H. Lee, S. Karkare, L. Cultrera, A. Kim, and I. V. Bazarov, *Rev. Sci. Instrum.* **86**, 073309 (2015).
- [18] B. Dunham *et al.*, *Appl. Phys. Lett.* **102**, 034105 (2013).
- [19] I. V. Bazarov, L. Cultrera, A. Bartnik, B. Dunham, S. Karkare, Y. Li, X. Xianghong, J. Maxson, and W. Roussel, *Appl. Phys. Lett.* **98**, 224101 (2011).
- [20] D. H. Dowell and J. F. Schmerge, *Phys. Rev. ST Accel. Beams* **12**, 074201 (2009).
- [21] S. Karkare and I. V. Bazarov, *Appl. Phys. Lett.* **98**, 094104 (2011).
- [22] M. Krasilnikov, in *Proceedings of FEL2006, BESSY, Berlin, Germany, 2006* (JACoW, Geneva, Switzerland, 2006), p. 583.
- [23] H. J. Qian, C. Li, Y. C. Du, L. X. Yan, J. F. Hua, W. H. Huang, and C. X. Tang, *Phys. Rev. ST Accel. Beams* **15**, 040102 (2012).
- [24] W. E. Spicer, *Phys. Rev.* **112**, 114 (1958).
- [25] T. Vecchione, D. Dowell, W. Wan, J. Feng, and H. A. Padmore, in *Proceedings of FEL2013, New York, NY, 2013* (JACoW, Geneva, Switzerland, 2013), p. 424.
- [26] S. Schubert, M. Ruiz-Osés, I. Ben-Zvi, T. Kamps, X. Liang, E. Muller, K. Müller, H. Padmore, T. Rao, X. Tong, T. Vecchione, and J. Smedley, *APL Mater.* **1**, 032119 (2013).
- [27] F. Zhou, A. Brachmann, F.-J. Decker, P. Emma, S. Gilevich, R. Iverson, P. Stefan, and J. Turner, *Phys. Rev. ST Accel. Beams* **15**, 090703 (2012).
- [28] W. J. Engelen, M. A. van der Heijden, D. J. Bakker, E. J. D. Vredenburg, and O. J. Luiten, *Nat. Commun.* **4**, 1693 (2013).
- [29] J. Maxson, L. Cultrera, C. Gulliford, and I. Bazarov, *Appl. Phys. Lett.* **106**, 234102 (2015).
- [30] See, for example, the Hamamatsu FESCA-200 femtosecond streak camera.